Journal of Ceramic Processing Research. Vol. 25, No. 6, pp. 1060~1068 (2024)
(Received 2 October 2024, Received in revised form 14 December 2024, Accepted 14 December 2024)
https://doi.org/10.36410/jcpr.2024.25.6.1060

J O U R N A L O F
Ceramic Processing Research

Graphene oxide-nanocellulose-cellulose acetate mixed matrix membrane as an efficient separator for carbon dioxide from natural gas

Mingyue Wang[a,b,c], Qiang Wei[a,*], Dong Li[b] and Changwei Pang[c]
[a]*China University of Petroleum-Beijing at Karamay, Engineering College, Karamay, Xinjiang 834000, China*
[b]*Applied Technology Research Institute of Northeast Petroleum University, Daqing, Heilongjiang 163318, China*
[c]*China University of Petroleum, Russia central Asia Research Center, Beijing 102249, China*

Removing carbon dioxide (CO_2) from natural gas is essential for improving fuel quality, preventing pipeline corrosion, and enhancing energy efficiency. Membrane technology offers a selective and efficient method for CO_2 removal, ensuring natural gas meets industry standards. This process reduces greenhouse gas emissions, supporting cleaner and more sustainable energy production. In this study, Mixed-matrix membranes (MMMs) incorporating graphene oxide (GO) stabilized by nanocellulose fibers (NCF) within a cellulose acetate (CA) matrix were synthesized and evaluated for CO_2/CH_4 gas separation. The CA/NCF/GO-1 membrane, with 1 wt% GO, demonstrated optimal performance, achieving a CO_2 permeability of 77.8 Barrer and an ideal CO_2/CH_4 selectivity of 24.3. SEM and FT-IR analyses confirmed the uniform dispersion of GO and strong filler-polymer interactions. XRD revealed enhanced crystallinity with GO addition, while TGA indicated thermal stability, with decomposition temperatures ranging from 277 °C to 310 °C. Mechanical testing showed increased tensile strength (up to 60 MPa) with filler addition, though excessive GO (2 wt%) caused aggregation and highly reduced % elongation at break. Gas permeabilities decreased at higher feed pressures (5 bar), aligning with the dual-sorption model. The CA/NCF/GO-1 membrane demonstrated high stability over one week and approached Robeson's 2008 upper bound, highlighting its potential for industrial CO_2 separation.

Keywords: Mixed matrix membranes, Clean energy, Carbon dioxide separation, Graphene oxide.

Introduction

The separation and purification of natural gas, primarily methane, are crucial due to its role in fulfilling a significant portion of global energy demands, which continue to grow. Carbon dioxide (CO_2) constitutes about 10 to 30% of natural gas, and despite being classified as an inert gas, its presence has a notable impact on combustion efficiency, as well as on transportation, storage, and environmental concerns [1]. Therefore, CO_2 separation from natural gas is both necessary and essential. Various techniques, such as absorption, cryogenic distillation, and adsorption, are commonly used for CO_2 capture and separation. However, these traditional methods have limitations, including high capital costs, operational complexities, and restricted CO_2 loading capacities [2]. In recent years, membrane technology has gained an advantage over conventional methods like adsorption, absorption, and distillation, owing to its lower investment costs and energy consumption for gas separation. Additionally, membrane technology offers operational simplicity, compactness, and environmental benefits [3].

The efficiency and cost-effectiveness of the membrane gas separation process are heavily influenced by the properties of the membrane materials used. Various types of membranes, including ceramic, inorganic, and polymeric, have been employed for gas separation [4, 5]. Among these, polymeric membranes have gained significant attention and commercialization due to their advantages such as low cost, flexibility, and scalability [6]. Commonly used polymers for membrane fabrication include cellulose acetate (CA), polysulfone, polyimide, polyurethane, polyvinyl alcohol, polyvinyl amine, and other tailored polymers. Among these, CA membranes have been extensively studied for gas separation because of their biodegradable and hydrophilic nature, as well as their ease of functionalization to enhance desired properties [7]. However, pure CA membranes face limitations in achieving high permeability and selectivity beyond the Robeson's upper bound, primarily due to the trade-off between selectivity and permeability.

To enhance gas separation performance in polymeric membranes, inorganic particles in the micro or nano-size range can be integrated into the polymeric matrix. Mixed matrix membranes (MMMs) were developed by combining inorganic fillers with polymers to overcome the trade-off between permeability and selectivity, while

*Corresponding author:
Tel : +86 13261357667
Fax: +86 13261357667
E-mail: 15600597779@163.com

also bridging the gap with pure inorganic membranes [8]. A wide range of nanomaterials, including zeolites, metal-organic frameworks (MOFs), carbon nanotubes, graphene sheets, activated carbon, carbon molecular sieves, silica, and metal oxides, have been incorporated into polymeric matrices to create MMMs [9]. The inclusion of nanoparticles can disrupt the polymer chain structure, leading to an increase in fractional free volume (FFV), internal cavities, and defects. As a result, incorporating nanoparticles enhances both gas permeation and selectivity [10].

In recent years, extensive research has focused on the design and synthesis of new materials by incorporating inorganic nanoparticles into polymeric membranes. One of the latest strategies involves integrating two-dimensional (2D) nanomaterials, such as graphene and graphene oxide (GO), to enhance membrane performance in areas such as permeability, selectivity, strength, and hydrophilicity [11]. Well-dispersed graphene particles within the polymer matrix can reduce polymer density and alleviate chain compression. These materials present a promising approach for creating membranes with tailored pore structures and well-defined pore size distributions, significantly improving both permeability and selectivity. The shape, size, and dispersion of the fillers play a crucial role in influencing gas permeability through mixed matrix membranes (MMMs) [12].

Recently, there has been growing interest in fabricating membranes using nanocellulose due to their advantages in separation applications. Nanocellulose is an excellent substrate for membrane fabrication and holds significant potential as a replacement for petroleum-based polymers. In particular, nanocellulose have been used as a membrane matrix to disperse and support various inorganic components [13]. For gas separation, cellulose acetate (CA) membranes incorporated with nanosized cellulose fibrils serve as excellent matrices for incorporating GO. The abundant hydroxyl groups on nanocellulose facilitate cross-linking with GO and ensure proper dispersion within the CA matrix. Additionally, the entangled web-like structure of nanocellulose fiber helps reduce voids in the membranes. Although numerous studies have explored the fabrication of graphene-containing mixed matrix membranes (MMMs) [11], the combination of GO and nanocellulose in a CA matrix for gas separation membranes remains unexplored.

In the present study, we have developed cellulose acetate (CA) mixed matrix membranes (MMMs) incorporating GO and nanocellulose through a simple synthesis method. The GO provide micropores that facilitate efficient gas separation, while the nanocellulose ensures the uniform dispersion of the GO within the CA matrix, preventing the formation of non-selective voids. The fabricated MMMs were then characterized in terms of their structural, morphological, thermal, and mechanical properties. Additionally, the study examined the effect of varying GO loadings on the permeability and selectivity of gases such as CO_2 and CH_4, and evaluated the membranes' potential for natural gas separation.

Materials and Methods

Chemicals

Cellulose acetate (CA, 50,000 MW) was sourced from Shanghai Darui Fine Chemical Co. (Shanghai, China) Graphene oxide (GO) was purchased from the Sixth Element Materials Technology Co., Ltd (Changzhou, China). Nanocellulose fiber suspension was obtained from QiHong Company (Guangxi, China). Dimethyl formamide (DMF, 99.8%) was supplied by Kaitong Chemical Reagent Co., Ltd (Tianjin, China). High-purity methane (CH_4) and carbon dioxide (CO_2) gases (99.999%) were used in the study. All chemicals and reagents were of analytical grade and used without further purification.

Membrane fabrication

The mixed matrix membranes (MMMs) were fabricated using solution casting and solvent evaporation. A 5 wt% cellulose acetate (CA) solution was prepared by sonicating in DMF for 5 minutes, followed by 60 minutes of stirring. This was mixed with nanocellulose fibers (NCF) in an aqueous slurry (0.1 wt% of CA). Graphene oxide (GO) at concentrations of 0.5, 1, and 2 wt% was added to the CA/NCF mixture and sonicated for 20 minutes. The degassed solution was cast onto a glass plate, dried at room temperature for 24 hours, and at 60 °C for 6 hours. Control and composite membranes were labeled as CA, CA/NCF, and CA/NCF/GO (with varying GO wt%).

Membrane characterization

The mixed matrix membranes (MMMs) underwent characterization using various techniques. Thickness measurements were performed using a thickness gauge (Liuling Instrument Factory, Shanghai, China). Surface morphologies were examined via field emission scanning electron microscopy (FE-SEM, Hitachi S-3500 N, Japan). To enhance conductivity during SEM analysis, all membrane samples were sputter-coated with gold for approximately 60 seconds before testing. The functional groups present on the developed membranes were analyzed using Nicolet iS-50 FTIR spectroscopy (Thermo Scientific, USA). The spectra were recorded in the 400-4000 cm^{-1} range under transmission mode. Each spectrum was produced by averaging 32 scans for improved accuracy. The crystalline properties of the mixed matrix membranes (MMMs) were analyzed using X-ray diffraction (D8 A25 DaVinci XRD, Bruker, Germany) with Cu-Kα radiation. The analysis was conducted over a 2θ range of 5-50°, using a step size of 0.045° to ensure detailed characterization.

Thermogravimetric analysis (TGA) was conducted using a Perkin Elmer STA6000 instrument to assess the

thermal stability of the MMMs. The analysis was carried out under a nitrogen atmosphere with a heating rate of 10 °C/min, covering a temperature range from 30 °C to 600 °C to observe thermal behavior. The tensile strength of the membrane was evaluated using a SHIMADZU AGS-X series universal tensile strength testing machine, equipped to handle a maximum load of 50 kN. Testing followed ASTM standard D882-02, with a strain rate set at 0.5 mm/min to ensure accurate assessment of the fabricated membrane samples.

Gas permeation experiments

The permeation behavior of the developed MMMs was evaluated using pure CO_2 and CH_4 gases at ambient temperature and varying pressures (1-5 bar). The gas flow rate through the membrane was measured with a soap bubble flowmeter, which records the time taken for a bubble to move from zero to a certain level [14]. Prior to measurements, the setup was evacuated to remove any adsorbed gases or solvents. Each membrane was tested at least three times, with average readings reported. Permeability was calculated using the equation given below,

$$Pa = \frac{Ql}{A\Delta P}\frac{273.15}{T} \quad (1)$$

The equation contains the following parameters: Q (volumetric flow rate in cm^3/s), l (membrane thickness), A (effective surface area in cm^2), ΔP (transmembrane pressure in cm Hg), and T (temperature in Kelvin). The ideal gas selectivity for the tested gases was calculated based on the ratio of single gas permeabilities, using Eq. (2) as shown below.

$$\alpha\,(a/b) = \frac{Pa}{Pb} \quad (2)$$

Results and Discussion

Despite the advantages of the MMM-based separation process, numerous challenges must still be addressed to facilitate the large-scale industrial use of such membranes [15, 16]. One of the main challenges is understanding the transport of species through the membrane and how it is influenced by the intrinsic properties of the filler and matrix. Among other materials, 2D materials have garnered significant attention in gas separation processes [17]. These fillers have sheet-like structures with atomic-scale size and thickness, making them ideal for creating transport channels in gas separation membranes. Similarly, the barriers formed by these layered materials enable selective gas transfer through the membrane, either by size sieving or electrostatic repulsion. As a result, the design of nanochannels using 2D molecular sieve materials has generated significant interest and research efforts. The sheet-like fillers are either randomly distributed or tend to align (to varying degrees) parallel to the membrane surface once incorporated into the polymer matrix. This alignment disrupts the diffusion pathways, enhancing membrane selectivity by creating greater resistance to larger molecules [18].

While graphene oxide has garnered significant interest in the membrane community, a major challenge remains its compatibility and uniform distribution within the polymer matrix. Nanocellulose, a notable biopolymer, has drawn attention due to its distinctive properties. It is increasingly recognized as an effective dispersing agent for 2D materials in polymer matrices, owing to its unique combination of features that enhance composite performance [19]. Nanocellulose contains hydroxyl groups that facilitate strong interactions with both 2D materials and the polymer matrix. Its fibrillar structure also offers a large surface area for interacting with 2D materials, helping to prevent their aggregation through steric and electrostatic stabilization [19]. This study developed mixed-matrix membranes (MMMs) incorporating graphene oxide stabilized by nanocellulose fibers within a cellulose acetate (CA) matrix and evaluated the CO_2/CH_4 separation.

Membrane Morphology

The gas transport properties of MMMs are highly influenced by the structural morphology of the resulting membranes [20]. To study the dispersion of NCF and GO particles within the CA matrix, the morphologies of the pure CA membrane and the MMMs were examined using SEM. The findings are presented in Fig. 1. The SEM image of the pure CA membrane reveals a dense, smooth, and homogeneous surface without defects (Fig. 1a). With the addition of NCF, although particles are visible on the membrane's surface, it retains a uniform appearance due to the excellent compatibility of NCF with cellulose (Fig. 1b). Similarly, in membranes incorporating GO, the SEM images clearly demonstrate that graphene particles are evenly distributed throughout the CA matrix. At a GO loading of 0.5 wt%, the smooth surface of the CA membrane slightly transitions to an irregular texture, with some particles becoming visible (Fig. 1c). It is evident that GO-embedded MMMs create more free cavities compared to the pure CA membrane. Additionally, the synthesized membranes display a dense morphology with the presence of some voids. For gas separation applications, dense morphologies are generally preferred, as they offer superior separation performance compared to porous structures. As the GO content increases to 1 wt%, a greater number of irregular sites are observed on the membrane surface (Fig. 1d). The presence of GO leads to larger void spaces within the polymer matrix, enhancing the permeability of CO_2 and CH_4. However, at higher GO loadings (2 wt%), more particles tend to agglomerate on the surface of the MMMs (Fig. 1e). The surface properties of the fabricated membranes were found to vary with the amount of filler added. However, at higher concentrations, the

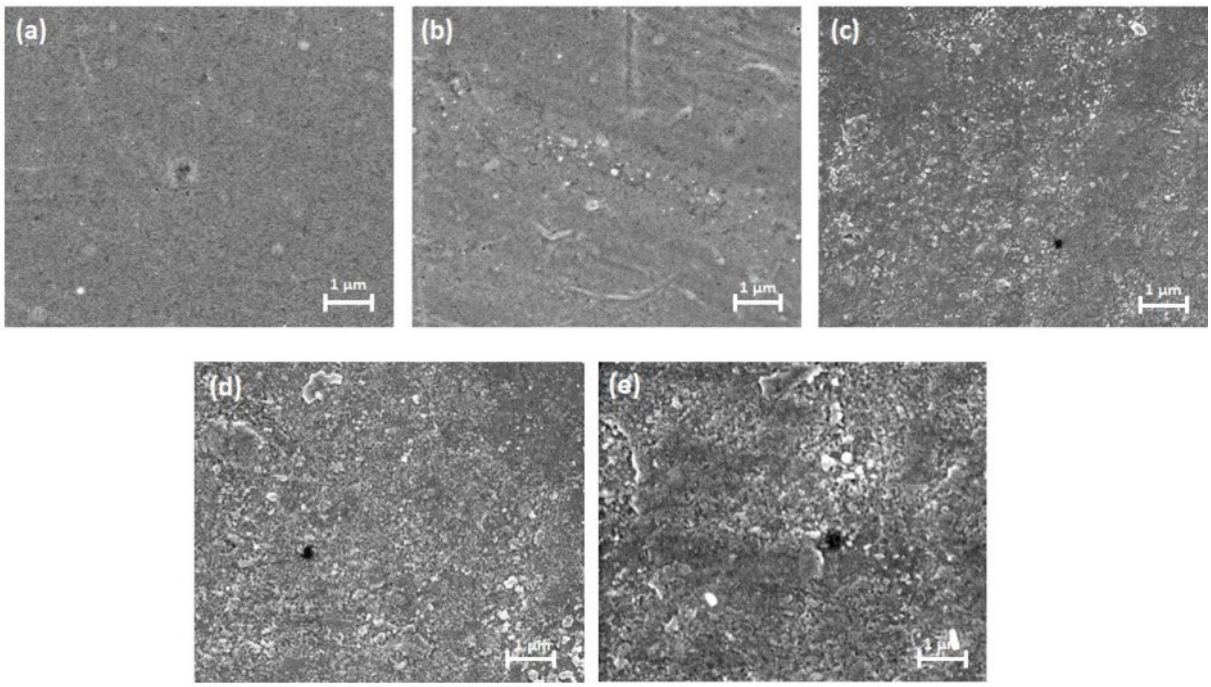

Fig.1. FE-SEM surface images of (a) pure CA, (b) CA/NCF, (c) CA/NCF-GO-0.5, (d) CA/NCF-GO-1, (e) CA/NCF-GO-2 MMMs.

aggregation of GO creates larger void spaces within the polymer matrix, potentially compromising the gas separation selectivity.

Structural properties

The impact of adding fillers (NCF and GO) on the chemical structure of the pure CA membrane was analyzed by comparing the FT-IR spectra of CA with those of the MMMs, as illustrated in Fig. 2a. The pure CA membrane exhibits an intense peak at 1734 cm^{-1} indicates the presence of the carbonyl group (C=O). While peaks at 2965 cm^{-1} and 1429 cm^{-1} represent $–CH_3$ asymmetric stretching and asymmetric deformation, respectively. Additionally, two other peaks, observed at 1216 cm^{-1} and 1031 cm^{-1}, are attributed to C-O-C and C-O stretching of acetate, respectively. The peak at 1367 cm^{-1} corresponds to C-CH_3 bending vibration. The peaks observed in Fig. 2a align closely with values reported in the literature [21]. With the addition of NCF to the CA membrane, the intensity of the peak around ~3300 cm^{-1} increases, the broad peak around ~3330 cm^{-1} corresponding to O-H stretching of NCF. A high peak intensity at 1640 cm^{-1} is associated with the interlayer stretching and bending vibration mode of molecular water in NCF. The incorporation of GO causes the broadening of peaks around ~1600 cm^{-1} and 1000 cm^{-1}. Additionally, the interactions between the filler and the polymer likely contribute to enhanced filler-polymer compatibility and the defect-free fabrication of the resulting MMMs. The FT-IR results confirm the

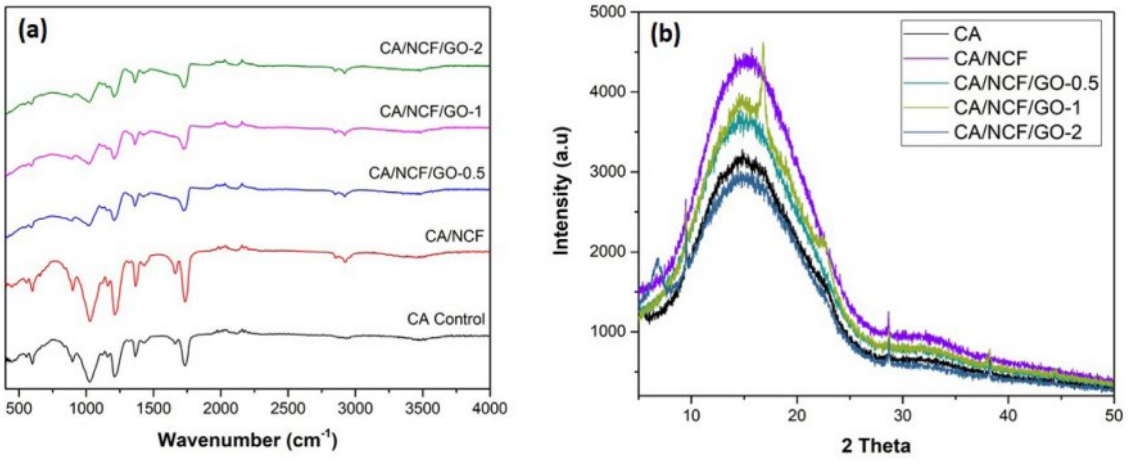

Fig. 2. (a) FT-IR spectra and (b) XRD spectra of MMMs.

successful fabrication of CA/NCF/GO MMMs.

The crystalline properties of the membranes were analyzed using XRD, with the results presented in Fig. 2b. The characteristic peaks of the pure CA membrane and MMMs are observed around 2θ = 10°-22°. The broad diffraction patterns indicate the glassy structure and semi-crystalline nature of membranes. The addition of NCF increases the intensity of crystalline peak of the membrane. The XRD spectra of GO containing MMMs didn't reveal any additional diffraction peaks. Generally, the incorporation of nanoparticles into a polymer alters the crystalline structure of the polymer phase [22]. Notably, the intensity of the broad XRD peak slightly increased with GO loading of 0.5 wt% and 1 wt%. At higher GO loading (2 wt%) the peak intensity decreased sharply, which indicates that the incorporation of higher GO concentrations breaks the pristine hydrogen bonding network in the membrane matrix and destroys the crystalline regions.

Thermal Properties

TGA was employed to assess the thermal properties of pure CA and MMM, aiming to evaluate the effect of filler loading on the polymer's stability. The TGA results for the CA and MMM membranes are presented in Fig. 3a. Three stages of weight degradation were observed in both pure CA and MMMs. In the first stage, all membranes showed approximately 10 wt% degradation, attributed to the loss of physically adsorbed H_2O and residual solvents. The major degradation occurred in the second stage (250-400 °C), with a weight loss of 80-90 wt% for all membranes, corresponding to the breakdown of the polymeric chains. The third stage involved the carbonization of the decomposed polymeric chains. The decomposition temperature of the pristine CA membrane is 310 °C. The thermal stability improves with the addition of NCF fillers, which is attributed to the inherent crystalline nature of NCF, with graphene absorbing a greater amount of heat. Meanwhile, the CA membrane with NCF begins decomposition at around 325 °C. For the MMMs with GO, the overall thermal stability is decreased compared to CA and NCF. The nano-fillers integrate into the polymer chains, hindering the inter-chain H-bond formation, which in turn decreases the energy required for polymer chain breakage [23]. Compared to the pristine membrane, the addition of 0.5, 1, and 2 wt% graphene decreased the decomposition temperature to 307 °C, 280 °C, and 277 °C, respectively (Fig. 3a). Similarly, the residue weight of the MMMs with GO was higher than that of pure CA, indicating that the thermal stability of GO in the MMMs is superior to that of matrix polymer. The residual mass of the membranes increases in the following order: CA (10%), CA/NC (12%), CA/NC/G 0.5 (15%), CA/NC/G 1 (17%), CA/NC/G 2 (18%). The overall thermal stability of the MMMs still meets the requirements of most CO_2 separation processes, which typically operate at temperatures below 100 °C.

Mechanical properties

To assess whether the mechanical strength of the prepared MMMs meets the requirements for practical applications, we conducted tests on their mechanical properties. The mechanical strength of pure CA and MMM was measured at an elongation rate of 0.5 $mm \cdot min^{-1}$. The resulting data are presented in the Fig. 3b. The pure CA membrane can withstand a maximum stress of 37±1.3 MPa and an elongation at break of 11 ±0.05. The mechanical properties significantly improved with the addition of 0.1 wt% NCF, achieving a tensile strength of 45±2.2 MPa and an elongation at break of 11±0.08. The tensile strength of the CA/NCF/GO membrane increases as the filler concentration rises from 0.5 to 2.0 wt%, while the elongation at break decreases with higher GO loading. Membrane samples with 0.5 wt% and 1.0 wt% filler can withstand stresses of up to 52±2.1 MPa and 57±1.8 MPa, respectively. At 2 wt% GO loading, the membrane attained a tensile strength of 61±1.7 MPa. However, increasing the GO loading results in a marked reduction in elongation at

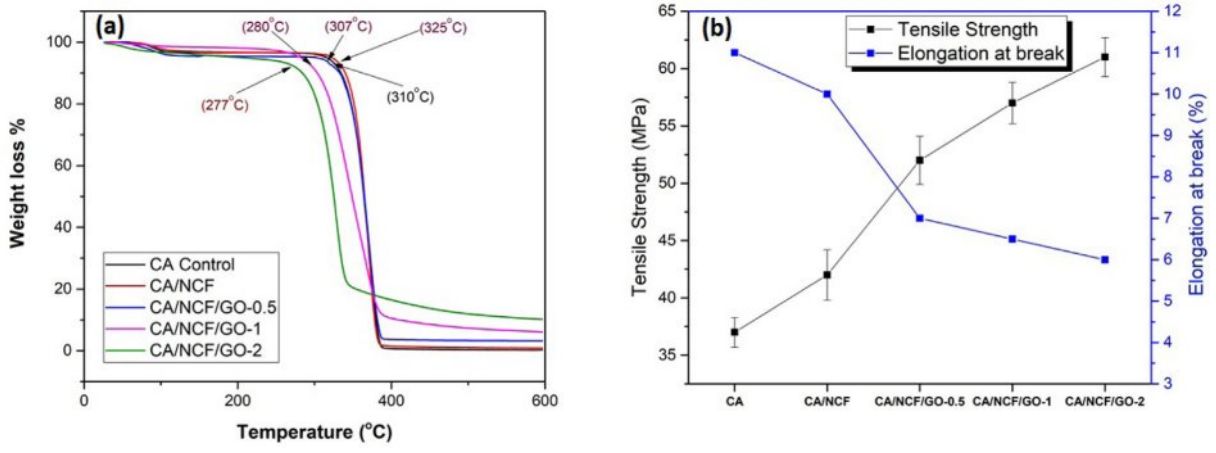

Fig. 3. (a) TGA graph and (b) mechanical properties of MMMs.

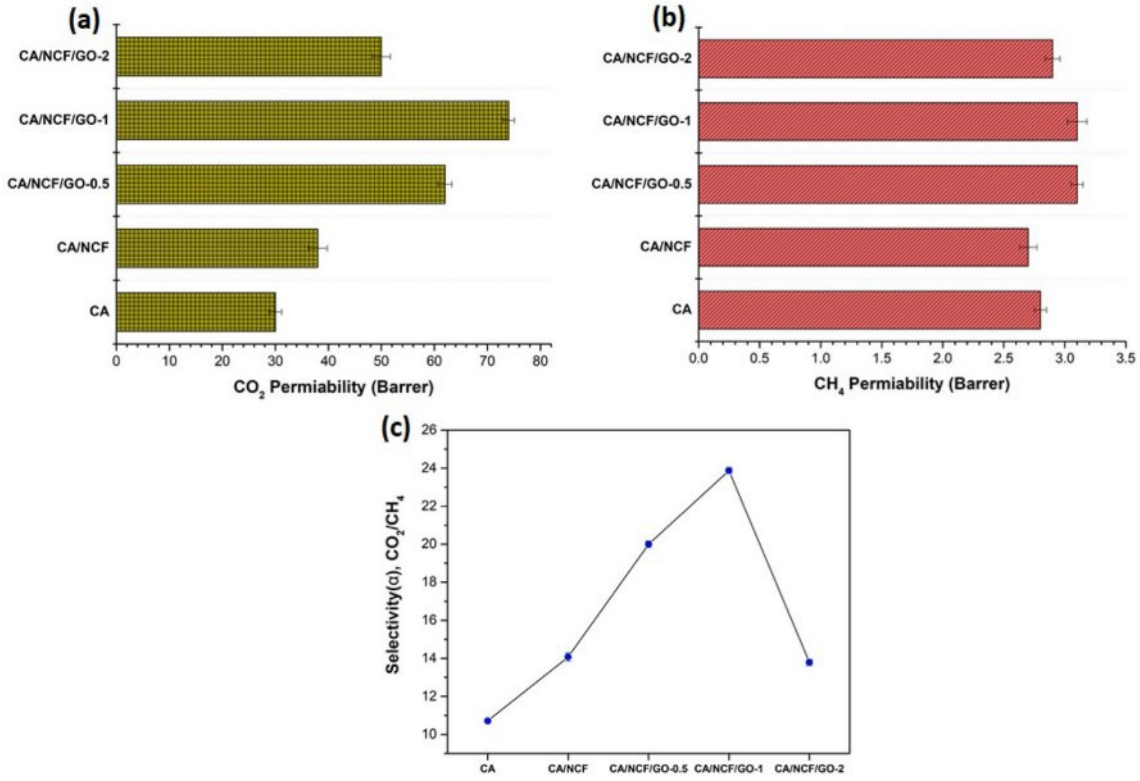

Fig. 4. Gas permeabilities of (a) CO_2 (b) CH_4 and (c) ideal gas selectivity of MMMs.

break, indicating that the membrane becomes stiffer due to the agglomeration of GO particles. The inclusion of GO particles within the CA chains enhances their stiffness, limiting chain orientation and imparting greater plasticity to the composite membrane [19]. As the GO concentration in the MMMs rises, the modulus exceeds that of the pristine CA membrane, resulting in the MMM exhibiting greater resistance to elastic deformation under applied stress.

Gas separation performance

The permeation of gases through a dense polymeric membrane follows the solution-diffusion mechanism [24]. In this process, the gas first dissolves at the membrane surface and then diffuses toward areas of lower concentration, driven by the concentration gradient. Gas diffusivity is a kinetic property, influenced by the kinetic diameter of the gases and the internal free volume within the polymer. In contrast, solubility is a thermodynamic factor, primarily affected by gas-polymer interactions and the condensability of the gas [25]. Generally, as the kinetic diameter increases (CO_2 < CH_4), gas diffusivity decreases (CO_2 > CH_4), with smaller gas molecules having a higher affinity for passing through the polymeric membrane than larger molecules [26]. Therefore, the kinetic diameter, gas solubility, and internal free volume within membranes are key factors controlling gas permeation. The disruption of polymer chains and the enhancement of internal free volume after filler incorporation are crucial strategies for improving the gas permeability of MMMs.

Effect of GO loading

To assess the CO_2 and CH_4 gas transport efficiency of the prepared MMMs, permeation tests were conducted at a temperature of 25 °C and a feed pressure of 1 bar. The gas flow rate was measured using a soap film flowmeter, an accurate device that determines flow by tracking the displacement of a soap film through a calibrated tube. Initially, we examined the effect of GO concentration on the permeability and selectivity of CO_2/CH_4 gases. As shown in Fig. 4, the pure gas permeability of CO_2 was higher than that of CH_4 for both pristine and GO-blended CA membranes. CO_2 exhibits higher diffusion and solubility coefficients due to its smaller kinetic diameter (CO_2 > CH_4). The results indicate that the gas permeabilities of pure CA membranes were 30 Barrer for CO_2 and 2.8 Barrer for CH_4, with an ideal CO_2/CH_4 selectivity of 10.7. The CA/NCF membrane exhibited a slight increase in gas permeability, with values of 38 Barrer for CO_2 and 2.7 Barrer for CH_4. The ideal selectivity of the CA/NCF membrane showed a higher value (14.7) compared to pure CA membrane.

The addition of 0.5 wt% GO (CA/NCF/GO-0.5) to the CA/NCF membrane increased CO_2 permeability to 62 Barrer, with a slight increase in CH_4 permeability (3.1 Barrer). The CA/NCF/GO-0.5 membrane exhibited an ideal selectivity value of 20. Subsequently, the CA/

NCF/GO-1 membrane showed further enhancement in CO_2 permeability, reaching 74 Barrer, while the CH_4 permeability remained unchanged (3.1 Barrer) with the 1 wt% GO loading. The ideal selectivity of the CA/NCF/GO-1 membrane improved, achieving a value of 23.8. Although the CO_2 permeability of the MMMs increased with 1 wt% GO loading, it decreased to 50 Barrer when the GO loading was further increased to 2 wt%. Meanwhile, the CO_2/CH_4 selectivity dropped to 17.2.

The CA/NCF/GO-1 MMMs exhibited higher gas permeabilities for all tested gases and enhanced gas selectivity (Fig. 4). The improved gas separation performance following the incorporation of GO is attributed to an increase in free voids and/or cavity volume caused by the disruption of the CA polymer chain. Additionally, the interactions between the filler and polymer through NCF promote uniform dispersion and better miscibility of the fillers within the CA matrix, contributing to the improved separation performance of the resulting MMMs. The enhancement in gas separation is further attributed to the high CO_2 absorption capacity of the MMMs, owing to the abundant polar groups present on the NCF [27].

Due to its smallest kinetic diameter, CO_2 exhibits higher gas permeation through the MMMs compared to CA, and this permeability increases further when the GO concentration rises from 0.5 to 1 wt%. However, at higher GO loadings (2 wt%), gas permeability decreases due to the agglomeration of GO platelets. Several factors may contribute to the reduced CO_2 permeability with increased nanoparticle concentration in the polymer. The incorporation of GO likely causes rigidification of the CA chains, which limits the mobility of the polymer chains, thereby hindering CO_2 permeability through the MMM [28].

CO_2/CH_4 selectivity values measure the membrane's ability to separate CO_2 and methane, specifically representing the ratio of the membrane's CO_2 permeability to its methane permeability. Membranes with high selectivity can effectively separate carbon dioxide while minimizing methane loss, leading to natural gas with higher purity. The MMM with 1 wt% graphene demonstrates improved CO_2/CH_4 separation, likely due to the well-dispersed GO platelets and the unique pore structure they create. Therefore, incorporating GO (up to 1 wt.%) creates additional molecular transport pathways, thereby improving CO_2 permeance and $CO_2/$

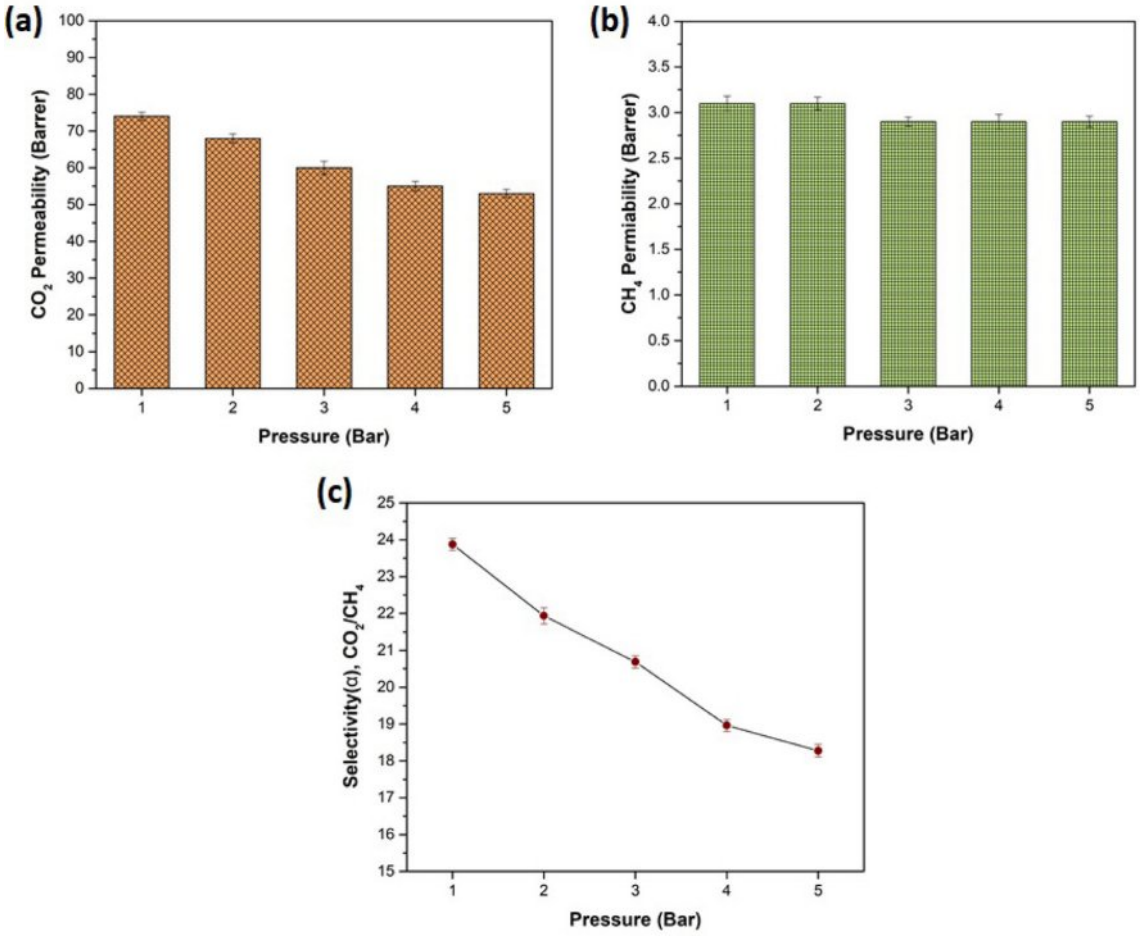

Fig. 5. Gas permeabilities of (a) CO_2 (b) CH_4 and (c) ideal gas selectivity of MMMs under different feed pressure.

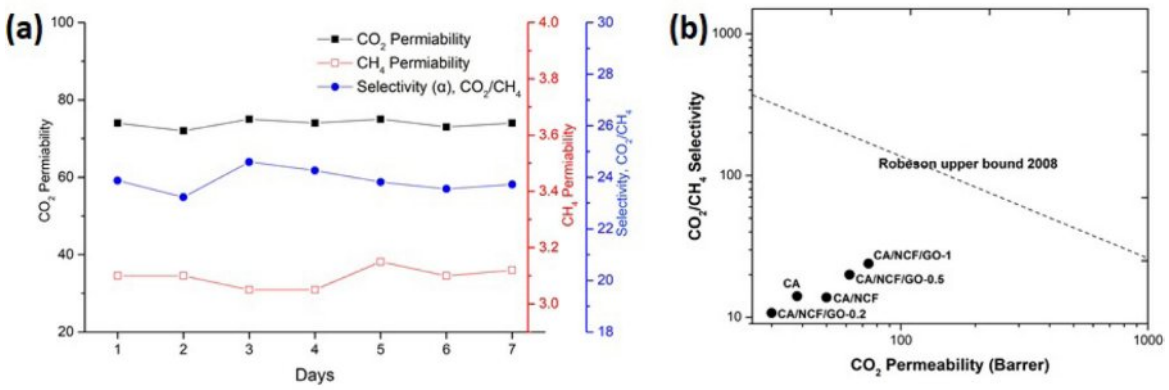

Fig. 6. (a) Long-term stability of CA/NCF/GO-1 membrane and (b) Comparison of CO_2/CH_4 separation performances of MMMs prepared in the current study with the Robeson upper bound plot (2008).

CH_4 selectivity.

Effect of feed pressure

Gas permeation tests for the selected CA/NCF/GO-1 membrane were conducted at feed pressures ranging from 1 to 5 bar. The impact of feed pressure on the gas permeabilities and selectivities of the CA/NCF/GO-1 membrane is presented in Fig. 5. The gas permeabilities of the MMMs for CO_2 and CH_4 decrease significantly with increasing pressure, which aligns with the typical behavior of glassy polymers and MMMs below the plasticization pressure [29]. For instance, the reduction in CO_2 permeability (28%) with an increase in pressure from 1 to 5 bar is more pronounced than the drop in CH_4 permeability. Consequently, the CO_2/CH_4 selectivity of the CA/NCF/GO-1 MMMs decreased to 18.2.

The decrease in gas permeability and selectivity can be attributed to two main factors. The primary factor is the compactness of the membrane, where an increase in feed pressure causes the polymer chains to shift from a loosely packed to a more tightly packed structure. This reduces the available free volume and restricts the diffusion of gas molecules through the membrane [29]. According to the dual-sorption model, the solubility of gases in glassy polymers initially increases with pressure, following Henry's Law. However, at higher pressures, the solubility levels off and becomes independent of pressure as the excess free volume (or voids) in the polymer reaches saturation, in accordance with Langmuir's adsorption behaviour [30]. Based on the observed results, a pressure of 1 bar is optimal for achieving high permeability and selectivity in the CA/NCF/GO-1 membrane.

Stability study

The CO_2/CH_4 separation efficiency of the CA/NCF/GO-1 MMMs was evaluated over a seven days separation experiment conducted at 1 bar pressure and 25 °C. The permeability deviation during the experiment was found to be less than 5%. As illustrated in figure 6a, the membrane's permeability and selectivity for CO_2/CH_4 separation remained consistent throughout the one-week experiment. This finding highlights the high stability of the synthesized MMMs and their promising potential for practical applications in CO_2 separation from natural gas.

Robeson's upper bound limit

Achieving a balance between the typically conflicting properties of gas permeability and selectivity poses a significant challenge in gas separation using conventional membranes [31]. For new membrane materials to find widespread industrial application, they must exhibit both high selectivity and high permeability simultaneously. Robeson's curve, a key benchmark for evaluating whether a membrane combines high selectivity and high permeability, is essential for assessing the potential of new membrane materials for large-scale industrial applications [32]. The separation performance of all fabricated membranes was evaluated against the 2008 Robeson upper bound curve, as shown in Fig. 6b. According to the Fig. 6b, the prepared MMMs did not surpass the 2008 Robeson upper bound. However, the separation performance of the CA/NCF/GO-1 MMMs approached the 2008 Robeson upper bound.

Conclusion

The study demonstrated that incorporating graphene oxide (GO) and nanocellulose (NC) into cellulose acetate (CA) membranes significantly enhances gas separation performance. Optimal GO loading (1 wt%) improved CO_2 permeability and CO_2/CH_4 selectivity due to well-dispersed fillers creating effective molecular transport pathways. Higher GO concentrations caused aggregation, reducing performance. Mechanical properties of the mixed-matrix membranes (MMMs) were superior to pristine CA, ensuring structural integrity under operating conditions. Stability tests confirmed consistent separation efficiency over time. Though the MMMs approached

Robeson's 2008 upper bound, further optimization is needed for surpassing industrial benchmarks. These findings highlight the potential of CA/NC/GO MMMs for efficient CO_2 separation from CH_4/CO_2 mix gas.

References

1. A. Imtiaz, M.H.D. Othman, A. Jilani, I.U. Khan, R. Kamaludin, J. Iqbal, and A.G. Al-Sehemi, Membranes 12[7] (2022) 646.
2. Z.Y. Yeo, T.L. Chew, P.W. Zhu, A.R.Mohamed, and S.-P. Chai, J. Nat. Gas Chem. 21[3] (2012) 282-298.
3. D. Chen, K. Wang, Z. Yuan, Z. Lin, M. Zhang, Y. Li, J. Tang, Z. Liang, Y. Li, L. Chen, L. Li, X. Huang, S. Pan, Z. Zhu, Z. Hong, and X. He, Carbon Capture Sci. Technol. 7 (2023) 100117.
4. Z. Li, Y. Ren, J. Hao, J. Xu, P. Yan, X. Zhang, and L. Li, J. Ceram. Process. Res. 25[3] (2024) 389-403.
5. P. Wu, Y. Xu, Z. Huang, and J. Zhang, J. Ceram. Process. Res. 16[1] (2015) 102-106.
6. G. Hazarika, and P.G. Ingole, Sci. Total Environ. 944 (2024) 173264.
7. Z. Bashir, S.S.M. Lock, N.e. Hira, S.U. Ilyas, L.G. Lim, I.S.M. Lock, C.L. Yiin, and M.A. Darban, RSC Adv. 14 (2024) 19560-19580.
8. T.-S. Chung, L.Y. Jiang, Y. Li, and S. Kulprathipanja, Prog. Polym. Sci. 32[4] (2007) 483-507.
9. S. Li, Y. Liu, D.A. Wong, J. Yang, Polymers 13 (2021) 2539.
10. M. Galizia, W.S. Chi, Z.P. Smith, T.C. Merkel, R.W. Baker, and B.D. Freeman, Macromolecules 50[20] (2017) 7809–7843.
11. A. Ali, R. Pothu, S.H. Siyal, S. Phulpoto, M. Sajjad, and K.H. Thebo, Mater. Sci. Energy Technol. 2 (2019) 83-88.
12. T.K. Junita, N. Syakir, F. Faizal, and Fitrilawati, ACS Omega 9 (2024) 20658-20669.
13. N. Li, J. Zheng, P. Hadi, M. Yang, X. Huang, H. Ma, H.W. Walker, and B.S. Hsiao, Membranes 9[6] (2019) 70.
14. A. Jamil, M. Zulfiqar, A. Momina, U. Arshad, S. Mahmood, I. Subhan, T. Iqbal, S. Rafiq, and M.Z. Iqbal, Adv. Polym. Technol. 12 (2020) 8855577.
15. R. Umapriya, J. Rohan, S.M. Vidyavathy, G. Thenmuhil, and G. Arthanareeswaran, J. Ceram. Process. Res. 21[3] (2020) 309-318.
16. R. Umapriya, S. Vidyavathy, M. Arthanareeswaran, G. Rohan, and A.R. Poorna, J. Ceram. Process. Res. 20[3] (2019) 291-300.
17. F. Zhou, Q. Dong, J.-T. Chen, B. Sengupta, J. Jiang, W.L. Xu, H. Li, S. Li, and M. Yu, Chem. Eng. J. 430 (2022) 132942.
18. J.M. Luque-Alled, M. Tamaddondar, A.B. Foster, P.M. Budd, and P. Gorgojo, ACS Appl. Mater. Interfaces 13 (2021) 55517-55533.
19. F. Pazani, M. Salehi Maleh, M. Shariatifar, M. Jalaly, M. Sadrzadeh, and M. Rezakazemi, Renew. Sustain. Energy Rev. 160 (2022) 112294.
20. Z. Niu, N. He, Y. Yao, A. Ma, E. Zhang, L. Cheng, Y. Li, and X. Lu, Chem. Eng. J. 494 (2024) 152912.
21. O. Mehmood, S. Farrukh, A. Hussain, M. Younas, Z. Salahuddin, E. Pervaiz, and M. Ayoub, Greenhouse Gas Sci. Technol. 11 (2021) 313-330.
22. C. Regmi, J. Azadmanjiri, V. Mishra, Z. Sofer, S. Ashtiani, K. Friess, Membranes 12[10] (2022) 917.
23. H.Z. Ferrari, F. Bernard, L. dos Santos, G. Dias, C. Le Roux, P. Micoud, F. Martin, and S. Einloft, Polym. Eng. Sci. 64[6] (2024) 2875-2893.
24. Y. Liu, N. Li, X. Cui, W. Yan, J. Su, and L. Jin, Membranes 12[12] (2022) 1274.
25. J.G. Wijmans, and R.W. Baker, The solution-diffusion model: a review. J. Membr. Sci. 107[1-2] (1995) 1-21.
26. Y. Zhang, J. Sunarso, S. Liu, and R. Wang, Int. J. Greenhouse Gas Control 12 (2013) 84-107.
27. Z. Wang, M. Li, X.F. Zhang, Y. Zhou, J. Yao, Cellulose 29 (2022) 1873-1881.
28. Y. Li, T.-S. Chung, C.Cao, and S.J. Kulprathipanja, Membr. Sci. 260[1-2] (2005) 45-55.
29. M.M. Rajpure, R.B. Mujmule, U. Kim, and H. Kim, Int. J. Hydrogen Energy 50[A] (2024) 615-628.
30. S. Kanehashi, and K. J. Nagai, Membr. Sci. 253[1-2] (2005) 117-138.
31. H.B. Park, J. Kamcev, L.M. Robeson, M. Elimelech, and B.D. Freeman, Science 356 (2017) eaab0530.
32. N. Panapitiya, S. Wijenayake, D. Nguyen, C. Karunaweera, Y. Huang, K. Balkus, I. Musselman, and J. Ferraris, Materials 9[8] (2016)643.